

Pyramidal Edge-maps based Guided Thermal Super-resolution

Honey Gupta and Kaushik Mitra, *Member, IEEE*

Abstract—Thermal imaging is a robust sensing technique but its consumer applicability is limited by the high cost of thermal sensors. Nevertheless, low-resolution thermal cameras are relatively affordable and are also usually accompanied by a high-resolution visible-range camera. This visible-range image can be used as a guide to reconstruct a high-resolution thermal image using guided super-resolution(GSR) techniques. However, the difference in wavelength-range of the input images makes this task challenging. Improper processing can introduce artifacts such as blur and ghosting, mainly due to texture and content mismatch. To this end, we propose a novel algorithm for guided super-resolution that explicitly tackles the issue of texture-mismatch caused due to multimodality. We propose a two-stage network that combines information from a low-resolution thermal and a high-resolution visible image with the help of multi-level edge-extraction and integration. The first stage of our network extracts edge-maps from the visual image at different pyramidal levels and the second stage integrates these edge-maps into our proposed super-resolution network at appropriate layers. Extraction and integration of edges belonging to different scales simplifies the task of GSR as it provides texture to object-level information in a progressive manner. Using multi-level edges also allows us to adjust the contribution of the visual image directly at the time of testing and thus provides controllability at test-time. We perform multiple experiments and show that our method performs better than existing state-of-the-art guided super-resolution methods both quantitatively and qualitatively.

Index Terms—thermal imaging, guided super resolution, pyramidal edge-maps, deep convolutional neural networks

I. INTRODUCTION

Far-infrared or thermographic imaging has many advantages over traditional visual-range imaging as it is less affected by illumination changes. It works well in extreme imaging conditions and has found applications in varied fields such as firefighting [1], gas leakage detection [2], automation [3]–[5] and many more but the high cost of thermal sensors restricts the extensive use of these cameras. Super-resolution(SR) techniques can further increase their applicability by simulating accurate high-resolution thermal images from low-resolution images captured from inexpensive thermal cameras. Most of the lower-end thermal cameras are accompanied by high-resolution visual-range cameras, and consequently, guided super-resolution seems to be the optimal solution to super-resolve the thermal images. However, due to the difference in the wavelength ranges of these sensors, the images can have different contents and texture, which can result in erroneous reconstructions.

Submitted for review on March 9, 2020.

Honey Gupta and Kaushik Mitra are with the Department of Electrical Sciences at Indian Institute of Technology Madras, Chennai 600036, India. (email: hn.gpt1@gmail.com, kmitra@ee.iitm.ac.in)

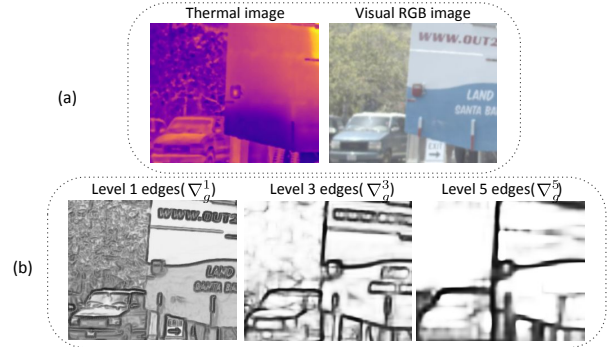


Fig. 1. (a) Texture mismatch between thermal and visible images due to multimodality. (b) Pyramidal edge-maps extracted from the visual image. Finer high-frequency(HF) details are present in Level-1 e.g. *car details*, but this level also contains the unwanted edges such as *texts*, which are absent in Level-5. This variation in HF details motivates us to use multilevel edge-maps.

The existing thermal super-resolution methods either perform single image SR [6]–[10] or visual-guided SR [11]–[17]. Among single thermal image SR, Choi *et al.* [9] suggested a shallow three-layer convolutional neural network(CNN). Zhang *et al.* [10] thereafter combined compressive sensing and deep learning techniques to perform infrared super-resolution. Among the guided thermal SR methods, Lee *et al.* [11] used brightness information for the visible-range images. Han *et al.* [12] proposed a guided SR method using CNN that extracts features from infrared and visible images and combines them using convolutional layers. Interestingly, most of the existing methods for depth [18]–[28] or hyperspectral [29]–[32] guided super-resolution have a similar backbone as the thermal guided-SR methods. They both use some variation of the Siamese network [33] to simultaneously extract information from both the low-resolution and guide images and merge them to get the super-resolved image.

A crucial part of super-resolution is to predict the high-frequency details correctly and the Siamese architecture along-with end-to-end training can help extract optimal high-frequency information. However, extracting optimal edges from the visual image belonging to the dissimilar domain is challenging, especially when the input image is of a very low-resolution, like the image captured from an inexpensive thermal cameras. The existing guided SR methods rely on the network to extract optimal information from the visual image and this can be difficult as it is scene dependent. Fig.1 shows one such case where optimal overlapping edges involve keeping some texture information, like the *structure of the car*, and simultaneously discarding some, like the *texts* on the truck. Moreover, texture or content mismatch can introduce artifacts

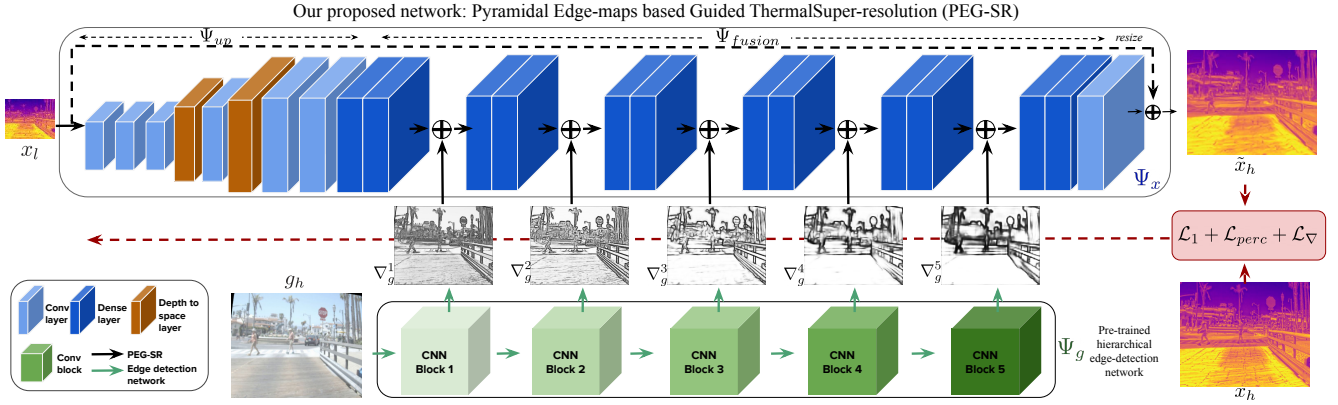


Fig. 2. Architecture of our proposed method: Pyramidal Edge-maps based Guided Thermal Super-resolution (PEG-SR) that utilises hierarchical edge information extracted from the guide visual image and merges this information into our thermal super-resolution network at different depths of the network. Our method progressively merges the texture to object-level information obtained from the visual-range image and provides a better way to perform guided super-resolution.

or blurred-edges in the super-resolved images. Ni *et al.* [34] proposed a method to utilise the edge-map and perform GSR but they have a similar vulnerability as their network estimates the optimized edges, which could be a source for the artifacts.

In this paper, we provide a systematic and holistic solution to deal with possible edge-mismatch caused due to multi-modality among the input images. Our method is motivated from the fact that layers at different depths of the network have different levels of features: going from fine texture information to object level information. Extracting edges at hierarchical perceptual scales or levels and integrating them in our tailored thermal super-resolution network can allow easier removal of the mismatched edges by the network and help reconstruct better high-frequency details. It also provides a way to adjust the guidance information provided to the network by choosing the levels of edges that are to feed to the SR network. In summary, the main contributions of this paper are:

- We propose a novel method for performing guided super-resolution by extracting pyramidal edge-maps from the visible image and integrating them into our thermal SR network in a hierarchical manner.
- We propose a way to adjust the contribution of the visual image according to factors like guide-noise, by adjusting the levels of edge-maps that are fed to the GSR network.
- We compare our model with existing state-of-the-art GSR methods and show that our method reconstructs the high-frequency details well and hence produces better result, both quantitatively and perceptually.

II. PYRAMIDAL EDGE-MAPS BASED GUIDED SUPER-RESOLUTION (PEG-SR)

The visible-range and thermal images have different contents due to differences in their wavelength ranges, as shown in Fig.1. Instead of following the conventional approach of using a Siamese network [12], [35], we design a new network which is better suited for the task of guided super-resolution (GSR). We know that the guide image has useful high-frequency details but these have to be extracted adaptively according to the input low-resolution thermal image. Non-optimality of the extracted high-frequency details from the visual image can lead to texture mismatch, which can further cause artifacts.

At the first glance, it seems that extracting the object-edges could be an ideal solution, but as one can observe from Fig.1, there are additional high-frequency details present in edge-maps at lower levels, *i.e.* levels 1 and 3 that are equally useful. To resolve this conundrum, we propose a systematic approach of using edge-maps extracted at pyramidal levels from the visual image and integrating them at appropriate layers of our SR network. In this way, the network can leverage high-frequency information in a hierarchical fashion and propagate the features as per the input low-resolution thermal image.

Figure 2 shows the architecture of our proposed method. We denote the low-resolution thermal, the high-resolution visible and ground-truth thermal images as x_l , g_h and x_h , respectively. Our network consists of two stages: one for thermal image super-resolution, denoted as Ψ_x and one for multi-level edge extraction from the visual image, denoted as Ψ_g .

Many existing edge-detection methods for a single image [36], [37] extract multi-level edges and merge them to obtain the desired object-edges. These methods inspired us to utilise the progressive nature of features in a convolutional neural network *i.e.* the relation that shallow layers have texture-like features and deeper layers have object-level features. They extract edges at different perceptual scales by taking output at different layers of the VGG [38] network, as also shown in Fig.2. Consequently, to obtain edges having visible-range information at different scales, we used the existing edge-extraction method [37] as Ψ_g . Ψ_g provides edge-maps at n pyramidal levels. We denote these edge-maps as $[\nabla_g^1, \nabla_g^2, \dots, \nabla_g^n]$, where $n = 5$ in case of [37].

Our super-resolution stage, Ψ_x , consists of two sub-networks: Ψ_{up} and Ψ_{fusion} . The first part of the network, denoted as Ψ_{up} , contains convolutional and upsampling layers. For a 2^k super-resolution, Ψ_{up} contains k depth-to-space layers. The output $X_1 = \Psi_{up}(x_l)$, is fed to the fusion sub-network Ψ_{fusion} . For n visual edge-maps, Ψ_{fusion} contains $n + 1$ dense-blocks [39], denoted as $[D_1, D_2, \dots, D_{n+1}]$. The pyramidal edges are added one-at-a-time after each dense-block in the increasing order of the receptive-field, *e.g.*, edge-map with fine-textures is added after the first dense-block and similarly for the rest of edge-maps:

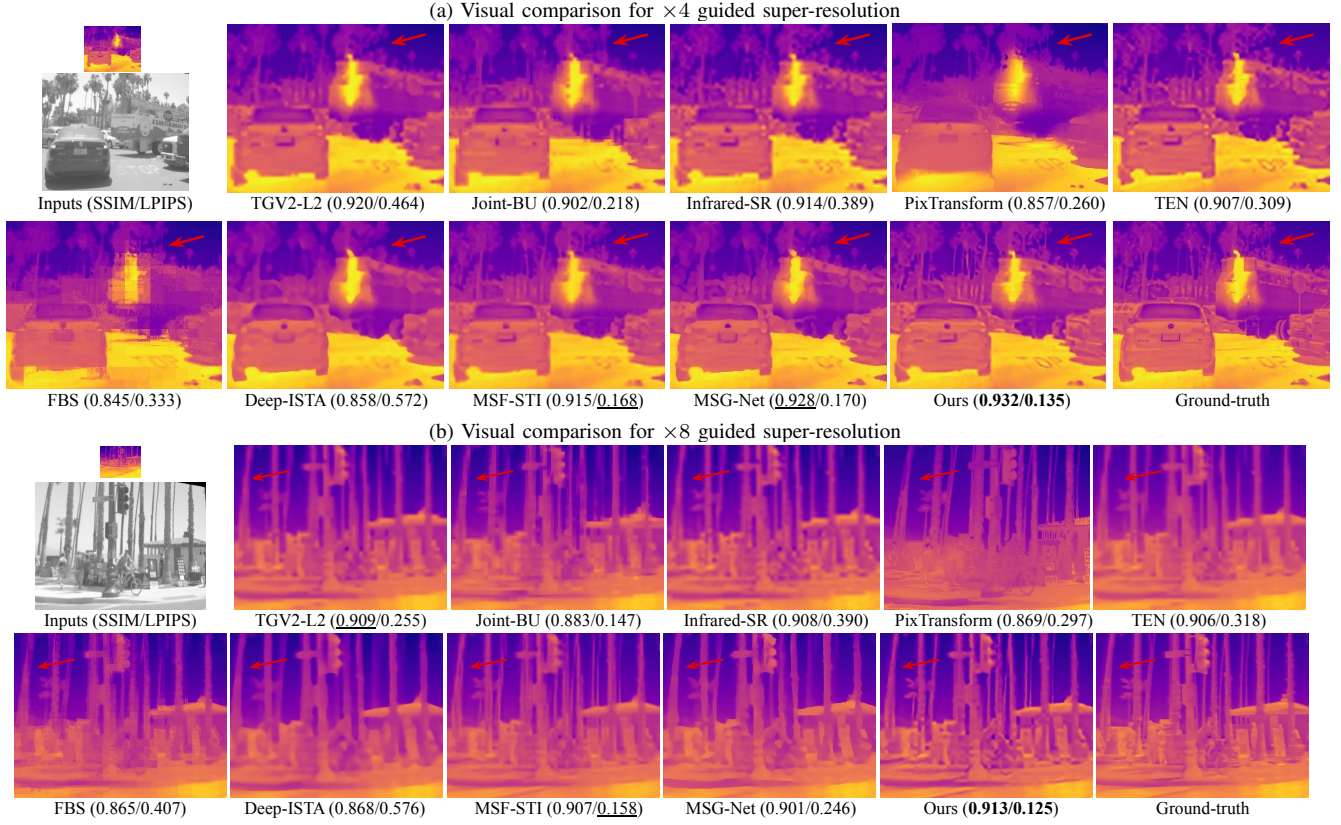


Fig. 3. Visual comparison on a sample image from FLIR-ADAS dataset. Our method reconstructs the high frequency details more accurately and thus produces better results as compared to existing GSR methods. This is also reflected by the high SSIM and low perceptual distance(LPIPS) values.

$$\begin{aligned}
 X_2 &= D_1(X_1) + \nabla_g^1 \\
 X_3 &= D_2(X_2) + \nabla_g^2 \\
 &\dots \\
 X_{n+1} &= D_n(X_n) + \nabla_g^n \quad (1)
 \end{aligned}$$

The final dense-block is followed by a convolutional layer and a skip-connection from the input for residual learning. We kept Ψ_x simple and avoided spatial attention or recurrent blocks to show that our proposed pyramidal edge-maps based GSR method works well even with a simple yet well-tailored convolutional neural network. The final output is $\tilde{x}_h = \Psi_x(x_l)$.

Loss functions. To learn the parameters of Ψ_x , our optimisation function contains three loss terms. The first is the reconstruction loss $\mathcal{L}_1 = \|\tilde{x}_h - x_h\|_1$ for supervised training. Secondly, we use the difference between VGG [38] features as a perceptual loss between the output and the ground-truth image. We denote this loss as \mathcal{L}_{perc} and VGG as Φ . Hence,

$$\mathcal{L}_{perc} = \|\Phi_{3_2}(\tilde{x}_h) - \Phi_{3_2}(x_h)\|_1 \quad (2)$$

We use the features from the convolutional layer 3_2 of Φ to compute \mathcal{L}_{perc} . Additionally, we also have a gradient loss $\mathcal{L}_\nabla = \|\nabla(\tilde{x}_h) - \nabla(x_h)\|_1$ to explicitly penalize loss of high frequency details. Hence, our overall loss function is:

$$\begin{aligned}
 \mathcal{L}(x_l, x_h, \Psi_x) &= \gamma_1 \times \mathcal{L}_1(\tilde{x}_h, x_h) \\
 &+ \gamma_{perc} \times \mathcal{L}_{perc}(\tilde{x}_h, x_h) + \gamma_\nabla \times \mathcal{L}_\nabla(\tilde{x}_h, x_h) \quad (3)
 \end{aligned}$$

After multiple experiments, we found the optimal values for γ_1 , γ_{perc} and γ_∇ to be 10, 1×10^{-4} and 1, respectively.

III. EXPERIMENTS AND RESULTS

To compare our method with the existing GSR methods, we performed qualitative and quantitative comparisons on two datasets: FLIR-ADAS [45] and CATS [46]. FLIR-ADAS contains unrectified thermal and visible image pairs having a resolution of 512×640 and 1600×1800 , respectively. Since the dataset does not contain any calibration images, we rectified one image pair manually and used the estimated relative transformation to rectify the rest of the images in the dataset. The CATS dataset, on the other hand, contains rectified thermal and visible images, both of dimensions 480×640 .

We used the blur-downscale degradation model [47] to create the low-resolution images. For the training-set, we down-sampled images with blur kernels $\in [0, 4]$ at a step of 0.5. For the FLIR-ADAS dataset, our training set contains 43830 downsampled image pairs and the test-set contains 1257 pairs. Whereas, in the CATS dataset, our training set contains 944 image-pairs and the test-set contains 50 pairs. Since CATS training-set is quite small, we used to it fine-tune the models pre-trained on FLIR-ADAS training-set and then tested them on CATS test-set. We perform experiments for $\times 4$ and $\times 8$ upsampling scales. For both cases, the input thermal-resolution is close to the resolution of many low-cost thermal cameras, like FLIR AX8 and FLIR One. For FLIR-ADAS, the low-resolution dimensions are 64×80 and for CATS, it is 60×80 .

A. Quantitative comparison.

We compare our method with 9 existing guided super-resolution methods: TGV2-L2 [23], FBS [40], Joint-BU [22],

TABLE I
COMPARISON OF GUIDED SUPER-RESOLUTION METHODS ON FLIR-ADAS AND CATS DATASET.

Method	FLIR-ADAS dataset						CATS dataset					
	$\times 4$			$\times 8$			$\times 4$			$\times 8$		
	PSNR	SSIM	LPIPS	PSNR	SSIM	LPIPS	PSNR	SSIM	LPIPS	PSNR	SSIM	LPIPS
TGV2-L2 [23]	28.77	0.892	0.422	26.42	0.821	0.399	32.17	0.938	0.225	31.55	0.951	0.303
FBS [40]	25.48	0.787	0.387	25.03	0.770	0.476	29.12	0.825	0.450	29.03	0.855	0.495
Joint-BU [22]	27.77	0.874	0.284	25.61	0.803	0.406	31.23	0.953	0.233	30.21	0.950	0.314
Infrared SR [12]	28.21	0.889	0.405	26.03	0.817	0.521	28.27	0.901	0.348	25.23	0.904	0.409
SDF [41]	28.70	0.875	0.321	26.72	0.819	0.363	32.56	0.941	0.246	31.91	0.948	0.319
MSF-SR [35]	29.21	0.901	0.200	27.92	0.835	0.249	29.37	0.830	0.415	27.97	0.811	0.418
MSG-Net [42]	29.46	0.897	0.184	27.29	0.827	0.296	31.56	0.964	0.177	32.83	0.957	0.270
PixTransform [43]	24.84	0.787	0.329	23.31	0.836	0.371	28.48	0.792	0.442	27.79	0.783	0.584
Deep-ISTA [44]	25.86	0.828	0.529	25.56	0.778	0.598	33.72	0.956	0.178	32.51	0.949	0.290
PEG-SR(Ours)	29.63	0.910	0.151	27.95	0.837	0.213	35.50	0.971	0.139	33.02	0.963	0.253

TABLE II
PERFORMANCE VARIATION WITH RESPECT TO HIERARCHY OF EDGE-MAPS FOR DIFFERENT NOISE LEVELS.

Model(Edge-levels)		No noise			$\sigma = 0.01$			$\sigma = 0.03$		
		PSNR	SSIM	LPIPS	PSNR	SSIM	LPIPS	PSNR	SSIM	LPIPS
(a)	PEGSR ₍₀₎ (Single image)	29.06	0.907	0.1755	29.06	0.907	0.1755	29.06	0.907	0.1755
(b)	PEGSR ₍₅₎	29.19	0.907	0.1733	29.10	0.907	0.1756	29.14	0.906	0.1759
(c)	PEGSR ₍₃₋₅₎	29.28	0.904	0.1793	29.26	0.906	0.1773	29.23	0.906	0.1785
(d)	PEGSR ₍₁₋₅₎ (Proposed)	29.64	0.910	0.1508	28.98	0.901	0.1803	28.88	0.899	0.1848
(e)	PEGSR ₍₁₋₅₎ (Retrained with noise)	29.33	0.912	0.1589	29.30	0.909	0.1715	29.28	0.908	0.1753

Infrared SR [12], SDF [41], MSF-SR [35], MSG-Net [42], Pix-Transform [43] and Deep-ISTA [44]. We use three metrics to quantitatively assess the methods' outputs: PSNR, SSIM and Perceptual distance(LPIPS) [48]. Among these, PSNR and SSIM are distortion-based metrics and can be biased towards blurred images. Hence, we also used LPIPS that computes the perceptual distance between the reconstructed and the ground-truth images. Higher PSNR, SSIM and lower LPIPS are better.

Table I shows the results for $\times 4$ and $\times 8$ upsampling scales. Most of the existing methods perform quite well in terms of distortion metrics but poorly in terms of the perceptual metric. However, our method outperforms the existing methods in terms of both metrics. Among the existing methods, MSG-Net [42] and MSF-SR [35] results are the closest to our method. PixTransform [43] and Deep-ISTA [44] are the most recent methods, yet they perform poorly as compared to the others, mostly due to edge-mismatch caused by multimodality.

B. Qualitative comparison.

We show the qualitative comparison of our method for $\times 4$ and $\times 8$ SR on FLIR-ADAS dataset in Fig.3. Most of the existing methods have blurred edges, especially in the case of $\times 8$ SR, which could be caused either due to very low-resolution of the input thermal images(60×80) or due to multimodality. Among the existing methods. MSF-STI, MSG-Net and Joint-BU results are considerably good, yet our method reconstructs high-frequency details more faithfully and has much sharper edges. It is evident perceptually as well as from the metrics that our results are closest to the ground-truth.

C. Variation with respect to noise and hierarchy of edge-maps

We performed experiments to analyze the contribution of different levels of edge-maps. Moreover, we also analyze the variation in performance with respect to the hierarchy of edge-maps when the input is a noisy visible image. To do this, we considered 3 variations of PEG-SR that contain

the same backbone SR network but separate sets of edge-maps as input. These models were trained on clean visual images but we tested them on edges extracted from noisy visual images containing added Gaussian noise with mean 0 and variance $\sigma = 0.01, 0.03$. Table II summarises the results from the performed study. PEGSR₍₀₎ is our model Ψ_x without any edge supervision; PEGSR₍₅₎ is Ψ_x network having only Level-5 edge-maps. Similarly, PEGSR₍₃₋₅₎ contains edges from Levels 3, 4 and 5; and PEGSR₍₁₋₅₎ is our proposed PEGSR network containing edges from Levels 1 to 5.

We observe that when the visual image contains no noise, the performance follows the order PEGSR₍₁₋₅₎ > PEGSR₍₃₋₅₎ > PEGSR₍₅₎ > PEGSR₍₀₎, which shows the effectiveness of using edge-maps at different levels. In case of noisy visual images, we observe that PEGSR₍₁₋₅₎ performs lower, mostly because the noise majorly affects lower level edge-maps *i.e.* 1 and 2. PEGSR₍₃₋₅₎ performs the best, followed by PEGSR₍₅₎ and PEGSR₍₀₎, which is consistent with the amount of guide information provided to the models. This shows that our model can be used to adjust the contribution of guide image and tune the network according to factors like noise. However, training with noisy visual images makes our proposed PEGSR network learn to adapt to the noise and hence, it performs much better, as shown in Table II(e).

IV. CONCLUSION

We proposed a hierarchical edge-based guided super-resolution algorithm (PEG-SR) that tackles multimodality and edge-mismatch between the input low-resolution thermal and high-resolution visible-range image in a systematic and holistic manner. Our method robustly combines multi-level edge information extracted from the visual image into our tailored thermal super-resolution network and consequently produces better high-frequency details. We showed that our results are better both perceptually and quantitatively than the existing state-of-the-art guided super-resolution methods.

REFERENCES

- [1] B. C. Arrue, A. Ollero, and J. M. De Dios, "An intelligent system for false alarm reduction in infrared forest-fire detection," *IEEE Intelligent Systems and Their Applications*, vol. 15, no. 3, pp. 64–73, 2000.
- [2] A. Prata and C. Bernardo, "Retrieval of volcanic ash particle size, mass and optical depth from a ground-based thermal infrared camera," *Journal of Volcanology and Geothermal Research*, vol. 186, no. 1-2, pp. 91–107, 2009.
- [3] S. Khattak, C. Papachristos, and K. Alexis, "Marker based thermal-inertial localization for aerial robots in obscure filled environments," in *International Symposium on Visual Computing*. Springer, 2018, pp. 565–575.
- [4] S. Khattak, C. Papachristos, and K. Alexis, "Keyframe-based direct thermal-inertial odometry," in *arXiv preprint arXiv:1903.00798*, 2019.
- [5] P. V. K. Borges and S. Vidas, "Practical infrared visual odometry," *IEEE Transactions on Intelligent Transportation Systems*, vol. 17, no. 8, pp. 2205–2213, 2016.
- [6] A. Panagiotopoulou and V. Anastassopoulos, "Super-resolution reconstruction of thermal infrared images," in *Proceedings of the 4th WSEAS International Conference on REMOTE SENSING*, 2008.
- [7] H. Jones and X. Sirault, "Scaling of thermal images at different spatial resolution: the mixed pixel problem," *Agronomy*, vol. 4, no. 3, pp. 380–396, 2014.
- [8] F. Almasri and O. Debeir, "Multimodal sensor fusion in single thermal image super-resolution," in *Asian Conference on Computer Vision*. Springer, 2018, pp. 418–433.
- [9] Y. Choi, N. Kim, S. Hwang, and I. S. Kweon, "Thermal image enhancement using convolutional neural network," in *2016 IEEE/RSJ International Conference on Intelligent Robots and Systems (IROS)*, Oct 2016, pp. 223–230.
- [10] X. Zhang, C. Li, Q. Meng, S. Liu, Y. Zhang, and J. Wang, "Infrared image super resolution by combining compressive sensing and deep learning," *Sensors*, vol. 18, no. 8, p. 2587, 2018.
- [11] K. Lee, J. Lee, J. Lee, S. Hwang, and S. Lee, "Brightness-based convolutional neural network for thermal image enhancement," *IEEE Access*, vol. 5, pp. 26867–26879, 2017.
- [12] T. Y. Han, Y. J. Kim, and B. C. Song, "Convolutional neural network-based infrared image super resolution under low light environment," in *2017 25th European Signal Processing Conference (EUSIPCO)*, Aug 2017, pp. 803–807.
- [13] F. Liu, P. Han, Y. Wang, X. Li, L. Bai, and X. Shao, "Super resolution reconstruction of infrared images based on classified dictionary learning," *Infrared Physics & Technology*, vol. 90, pp. 146–155, 2018.
- [14] C. Sun, J. Lv, J. Li, and R. Qiu, "A rapid and accurate infrared image super-resolution method based on zoom mechanism," *Infrared Physics & Technology*, vol. 88, pp. 228–238, 2018.
- [15] N. Yokoya, "Texture-guided multisensor superresolution for remotely sensed images," *Remote Sensing*, vol. 9, no. 4, p. 316, 2017.
- [16] P. Song, X. Deng, J. F. Mota, N. Deligiannis, P. L. Dragotti, and M. R. Rodrigues, "Multimodal image super-resolution via joint sparse representations induced by coupled dictionaries," *arXiv preprint arXiv:1709.08680*, 2017.
- [17] X. Chen, G. Zhai, J. Wang, C. Hu, and Y. Chen, "Color guided thermal image super resolution," in *2016 Visual Communications and Image Processing (VCIP)*. IEEE, 2016, pp. 1–4.
- [18] G. Riegler, D. Ferstl, M. R  ther, and H. Bischof, "A deep primal-dual network for guided depth super-resolution," *arXiv preprint arXiv:1607.08569*, 2016.
- [19] W. Zhou, X. Li, and D. Reynolds, "Guided deep network for depth map super-resolution: How much can color help?" in *2017 IEEE International Conference on Acoustics, Speech and Signal Processing (ICASSP)*. IEEE, 2017, pp. 1457–1461.
- [20] C. Guo, C. Li, J. Guo, R. Cong, H. Fu, and P. Han, "Hierarchical features driven residual learning for depth map super-resolution," *IEEE Transactions on Image Processing*, 2018.
- [21] J. Xie, R. Feris, and M.-T. Sun, "Edge-guided single depth image super resolution," vol. 25, no. 1, pp. 428–438, Jan 2016.
- [22] J. Kopf, M. F. Cohen, D. Lischinski, and M. Uyttendaele, "Joint bilateral upsampling," in *ACM Transactions on Graphics (ToG)*, vol. 26, no. 3. ACM, 2007, p. 96.
- [23] D. Ferstl, C. Reinbacher, R. Ranftl, M. R  ther, and H. Bischof, "Image guided depth upsampling using anisotropic total generalized variation," in *Proceedings of the IEEE International Conference on Computer Vision*, 2013, pp. 993–1000.
- [24] D. Zhou, R. Wang, X. Yang, Q. Zhang, and X. Wei, "Depth image super-resolution reconstruction based on a modified joint trilateral filter," *Royal Society open science*, vol. 6, no. 1, p. 181074, 2019.
- [25] Y. Li, J. Sun, B. Wang, and Y. Zhao, "Depth super-resolution using joint adaptive weighted least squares and patching gradient," in *2018 IEEE International Conference on Acoustics, Speech and Signal Processing (ICASSP)*. IEEE, 2018, pp. 1458–1462.
- [26] K. Hayat, "Multimedia super-resolution via deep learning: A survey," *Digital Signal Processing*, vol. 81, pp. 198–217, 2018.
- [27] S. Yu, H. Lan, and C. Jung, "Intensity guided depth upsampling using edge sparsity and super-weighted l_0 gradient minimization," *IEEE Access*, vol. 7, pp. 140553–140565, 2019.
- [28] J. Ye, M. Gao, Y. Yang, Q. Cao, and Z. Yu, "Super-resolution reconstruction of depth image based on edge-selected deep residual network," in *2019 IEEE 16th International Conference on Networking, Sensing and Control (ICNSC)*. IEEE, 2019, pp. 121–125.
- [29] F. Lahoud, R. Zhou, and S. S  strunk, "Multi-modal spectral image super-resolution," in *European Conference on Computer Vision*. Springer, 2018, pp. 35–50.
- [30] Z. Shi, C. Chen, Z. Xiong, D. Liu, Z.-J. Zha, and F. Wu, "Deep residual attention network for spectral image super-resolution," in *European Conference on Computer Vision*. Springer, 2018, pp. 214–229.
- [31] H. Kwon and Y.-W. Tai, "Rgb-guided hyperspectral image upsampling," in *Proceedings of the IEEE International Conference on Computer Vision*, 2015, pp. 307–315.
- [32] M. Shoeiby, A. Robles-Kelly, R. Timofte, R. Zhou, F. Lahoud, S. S  strunk, Z. Xiong, Z. Shi, C. Chen, D. Liu *et al.*, "Pirm2018 challenge on spectral image super-resolution: methods and results," in *Proceedings of the European Conference on Computer Vision (ECCV)*, 2018, pp. 0–0.
- [33] L. Bertinetto, J. Valmadre, J. F. Henriques, A. Vedaldi, and P. H. Torr, "Fully-convolutional siamese networks for object tracking," in *European conference on computer vision*. Springer, 2016, pp. 850–865.
- [34] M. Ni, J. Lei, R. Cong, K. Zheng, B. Peng, and X. Fan, "Color-guided depth map super resolution using convolutional neural network," *IEEE Access*, vol. 5, pp. 26666–26672, 2017.
- [35] F. Almasri and O. Debeir, "Multimodal sensor fusion in single thermal image super-resolution," *arXiv preprint arXiv:1812.09276*, 2018.
- [36] S. Xie and Z. Tu, "Holistically-nested edge detection," in *Proceedings of IEEE International Conference on Computer Vision*, 2015.
- [37] Y. Liu, M.-M. Cheng, X. Hu, J.-W. Bian, L. Zhang, X. Bai, and J. Tang, "Richer convolutional features for edge detection," *IEEE Trans. Pattern Anal. Mach. Intell.*, vol. 41, no. 8, pp. 1939 – 1946, 2019.
- [38] K. Simonyan and A. Zisserman, "Very deep convolutional networks for large-scale image recognition," *arXiv preprint arXiv:1409.1556*, 2014.
- [39] G. Huang, Z. Liu, L. Van Der Maaten, and K. Q. Weinberger, "Densely connected convolutional networks," in *Proceedings of the IEEE conference on computer vision and pattern recognition*, 2017, pp. 4700–4708.
- [40] J. T. Barron and B. Poole, "The fast bilateral solver," *ECCV*, 2016.
- [41] B. Ham, M. Cho, and J. Ponce, "Robust image filtering using joint static and dynamic guidance," in *Proceedings of the IEEE Conference on Computer Vision and Pattern Recognition (CVPR)*, IEEE, 2015.
- [42] T.-W. Hui, C. C. Loy, and X. Tang, "Depth map super-resolution by deep multi-scale guidance," in *Proceedings of European Conference on Computer Vision (ECCV)*, 2016, pp. 353–369. [Online]. Available: http://mmlab.ie.cuhk.edu.hk/projects/guidance_SR_depth.html
- [43] R. d. Lutio, S. D'Arconco, J. D. Wegner, and K. Schindler, "Guided super-resolution as pixel-to-pixel transformation," in *Proceedings of the IEEE International Conference on Computer Vision*, 2019, pp. 8829–8837.
- [44] X. Deng and P. L. Dragotti, "Deep coupled ista network for multimodal image super-resolution," *IEEE Transactions on Image Processing*, vol. 29, pp. 1683–1698, 2019.
- [45] FLIR. (2018) Advanced driver assistance systems dataset. [Online]. Available: <https://www.flir.in/oem/adas/>
- [46] W. Treible, P. Saponaro, S. Sorensen, A. Kolagunda, M. O'Neal, B. Phelan, K. Sherbondy, and C. Kambhampettu, "Cats: A color and thermal stereo benchmark," in *Proceedings of the IEEE Conference on Computer Vision and Pattern Recognition*, 2017, pp. 2961–2969.
- [47] K. Zhang, W. Zuo, and L. Zhang, "Learning a single convolutional super-resolution network for multiple degradations," in *Proceedings of the IEEE Conference on Computer Vision and Pattern Recognition*, 2018, pp. 3262–3271.
- [48] R. Zhang, P. Isola, A. A. Efros, E. Shechtman, and O. Wang, "The unreasonable effectiveness of deep features as a perceptual metric," in *CVPR*, 2018.